Journal of Luminescence 131 (2011) 1594–1598

Contents lists available at ScienceDirect

Journal of Luminescence

journal homepage: www.elsevier.com/locate/jlumin

Enhanced photoluminescence of conjugated polymer thin films on nanostructured silver

Michael S. Griffo [a], Sue A. Carter [a,*], Amanda L. Holt [b]

[a] Physics Department, University of California, Santa Cruz, 1156 High Street, Santa Cruz, CA 95064, United States
[b] Collaborative Biotechnologies, University of California, Santa Barbara, Marine Biotechnology Building, Santa Barbara, CA 93106, United States

ARTICLE INFO

Article history:
Received 6 July 2010
Received in revised form
14 February 2011
Accepted 18 February 2011
Available online 21 March 2011

Keywords:
Polymer
Nanoparticles
Nanostructure
Photoluminescence
Surface enhanced fluorescence
Plasmonics

ABSTRACT

Photoluminescence of a conjugated polymer in the presence of surface plasmons on metallic nanoparticles is studied. A layered device structure was constructed that enabled control over nanoparticle diameter and separation between the polymer and nanoparticles layers. The dependence of the surface plasmon evanescent field and energy transfer has been investigated with the largest enhancement in photoluminescence observed at a 40 nm distance separation between the fluorophore and the surface plasmon. A spectrum of surface plasmon resonances ranging from the emission to the absorption energies of the conjugated polymer revealed largest enhancements when the resonance was tuned to the conjugated polymer emission energy. At peak photoluminescence the maximum photoluminescent enhancement was found to be 5.6 times of the photoluminescence of the control structure and the total integrated enhancement was 5.9 times.

1. Introduction

Recently, interest in electromagnetic coupling with the surface plasmon (SP) has increased due to advances in nanoscale fabrication techniques and an emergence of a large variety of applications. In the last decade, research has shown large enhancements in ultra-sensitive sensors [1], fluorescence [2–4], and diodes [5] due to the proximal effects plasmons have on materials. A plethora of researchers are actively pursuing increases in light absorption in silicon based photovoltaics [6] and surface enhanced fluorescence (SEF) of dyes [7,8] using SPs but only a few have begun to probe the differences in photoluminescence (PL) of conjugated polymers and organic dyes [9–12]. Given the importance of the fluorescent semiconducting polymers for applications such as light emitting diodes, solar cells [13], and luminescent solar concentrators [14], it is of interest to understand the large ratio of enhancements in dyes compared to conjugated polymers and the optimal distance dependence between the SP and the fluorescing molecule.

Conjugated polymer PL should be strongly affected by the SP because the fluorescent molecule's excitation intensity is correlated with the electromagnetic field and the radiative decay efficiency is related to the decay rates, both of which SPs have an effect on. The PL enhancement (Y) at the weak excitation limit is dependent upon the radiative decay efficiency (Z) and the excitation intensity (L), which is related to the electromagnetic field intensity, and can be expressed as [15]

$$Y = |L(\omega_{ex})|Z(\omega_{ft}). \quad (1)$$

At the SP energy resonance, electromagnetic fields have been shown [16] to be amplified by factors larger than 10^4; thus enhancement in conjugated polymer PL can be realized by optimizing the overlap of the SP resonance and the fluorophore band gap excitation and emission wavelengths [17].

A balance between maximizing the SP evanescent electromagnetic field across the polymer and minimizing the quenching, due to energy transfer from the fluorophore to the nanoparticle (NP), must be met for optimization of the SEF. Metallic quenching of fluorescent materials in a planar geometry is well understood by previous work from Becker et al.[18] and Drexhage [19] who have shown the effects of a solid silver (Ag) plane in proximity to a fluorescent polymer layer. This work shows the critical distance dependence that is encountered when attempting to use a smooth planar array of Ag NPs to source an enhanced field.

A decrease in exiton lifetime and an increase in fluorescent quantum yield of a dilute suspension of conjugated polymers have been observed and attributed to SEF effects [11]. This effect was observed by Liu et al. [12] for a solution containing a mixture of gold NPs and poly[2-methoxy-5-(2′-ethylhexyloxy)-p-phenylene vinylene] (MEH-PPV). Although an overall increase in quantum yield and a decrease in exiton lifetime were observed the energy transfer between the NPs and the MEH-PPV caused quenching, which resulted in an overall decrease in performance. This interesting

* Corresponding author. Tel.: +1 831 335 7595.
E-mail addresses: mgriffo@physics.ucsc.edu (M.S. Griffo), sacarter@ucsc.edu (S.A. Carter).

0022-2313/$ - see front matter © 2011 Elsevier B.V. All rights reserved.
doi:10.1016/j.jlumin.2011.02.040

study has shown that enhancement in the fluorescence of MEH-PPV is possible if quenching is mitigated and SEF is maximized. However, the limitations of this study leave room for further investigation. An experiment with control over the distance between NPs and MEH-PPV would allow us to properly evaluate the quenching distance dependence in the presence of SEF. A thorough study of a range of SP resonances should also be performed to ensure that SEF is optimized for maximum enhancement. In addition, due to the high quantum efficiency of dilute suspensions of MEH-PPV a study should be performed where interchain coupling is higher and so the potential for enhancement is greater.

We report on a study of MEH-PPV thin films in the presence of tuned SPs that has several advantages compared to previous studies. The distance between NPs and MEH-PPV is controlled with an optically transparent dielectric thin film, which allows us to analyze the quenching distance dependence with SEF effects. This experimental design also allows us to control the thickness of the MEH-PPV thin film such that evanescent fields from the SP are able to penetrate through the entire thin film, which enables proper characterization of the investigated effects. In addition, SEF is optimized through tuning of the SP resonances over a range of wavelengths extending from the peak absorption to the peak emission wavelengths of MEH-PPV. Finally, interchain coupling is high for MEH-PPV thin films with a large difference in reported in-solution quantum efficiency and thin film quantum efficiency, 0.85 and 0.15, respectively [20]. This low thin film quantum efficiency allows for easier examination of enhancement effects. This study results in an enhancement of light emission from MEH-PPV through optimization of SEF and the mitigation of quenching effects.

2. Experiment

Three different types of device structures were created, as shown in Fig. 1. The first had the simplest structure—MEH-PPV spun cast onto a Corning 1737 glass substrate. The second type had a thin Ag mirror deposited on a glass substrate with a lithium fluoride (LiF) spacer layer separating a spun cast MEH-PPV layer from the Ag mirror. The third device type is similar to the mirror devices but in place of the mirror an Ag NP layer was fabricated.

Ag deposition onto Corning 1737 glass substrates was performed by thermal evaporation at 7×10^{-6} Torr. For the NP devices the Ag films were then annealed in air at 125, 175, 225, and 350 °C for 6 min at each step with a 6 min cooling period between steps. This four-stage anneal process allowed the particles to coalesce from varied morphologies to a film of spheroids with minimal diameter dispersion [6]. For the mirror and NP devices, LiF was then deposited by thermal evaporation before a spun cast thin film of MEH-PPV completed the device structure.

In this study the Ag deposition thickness ranged from 5 to 20 nm, the LiF film thickness was varied from 5 to 110 nm, and the thickness of the MEH-PPV was constant at 40 nm. MEH-PPV, purchased from American Dye Source, had a molecular weight of 629k and a polydispersity of 2:1. All thermal evaporation was controlled by a calibrated crystal quartz monitor and all thicknesses were confirmed using Atomic Force Microscopy (AFM). Each substrate has an average area of $\sim$6.45 cm^2. Controls were fabricated using the same techniques without the evaporation of Ag.

At each stage of fabrication, analysis of the Ag, LiF, and MEH-PPV layers was performed using AFM for characterization of surface morphology and thicknesses. A n&k Transmission Reflection Spectrometer was used for characterization of the absorptance for specific layers of the device and a Perkin Elmer Photoluminescence Spectrometer (LS-45) was used to measure the PL of the completed devices. Light was incident upon the MEH-PPV at 30° from normal and emitted light was detected at 54° from normal. We did not observe any significant angle dependence of the photoluminescence from the neat MEH-PPV films. Several data acquisitions were performed at different sample orientations with several samples to check for variation and ensure uniformity.

3. Results and discussion

Ag deposition was varied from 5 to 20 nm in 5 nm increments. Annealing of the Ag layer resulted in a homogeneous and dense NP layer with SP resonance peaks ranging in energy from the

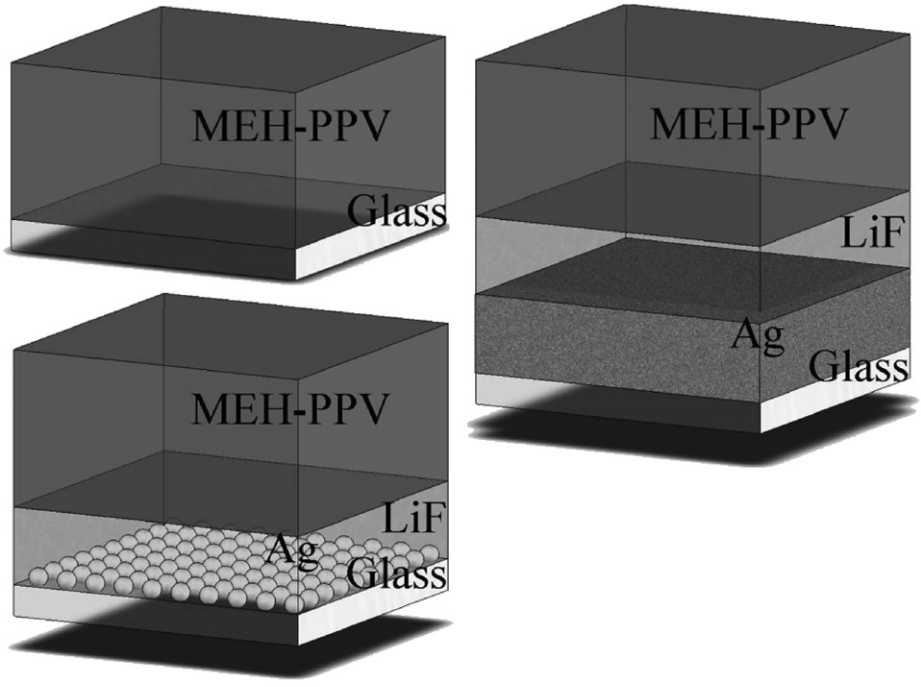

Fig. 1. Schematic diagrams of the PL device structures. Device (1) is only MEH-PPV on glass, device (2) contains a solid Ag layer, and device (3) features on Ag NP layer.

absorption to the emission peaks of MEH-PPV. Surface analysis revealed that RMS surface roughness is an accurate estimation of particle diameter and that the elliptical spheroidal NPs had axial ratios near 1.7. The axial ratio achieved is advantageous compared to spheroidal NPs for this experiment because, as previously reported, there is an increase in the SP excitation with increasing eccentricity of the NPs [21]. Table 1 details the relationship between Ag deposition and the average of the resulting NP diameters after annealing.

With non-spherical NP structures, the polarization of light used to excite the SPs is critical. Hence PL and transmission data were acquired at four different rotational orientations of the device, where the device was rotated about an axis perpendicular to the surface. These data confirmed that the devices were rotationally independent which was expected because of the random orientation of NPs in the AFM measurements, Fig. 2, and the expected radial orientation of spun cast MEH-PPV thin films.

Although previous studies have demonstrated control over SP characteristics from deposition of Ag NPs [22] it is necessary to comment on the characteristics and limitations of the technique used in this experiment. The absorptance spectra of Ag layers change with evaporation thickness and heat treatment as shown in Fig. 3. The dashed black curves show the spectra of the deposited Ag layers whereas the solid gray curves exhibit the spectra of the Ag layers after formation of NPs. Two plasmon modes can be seen after NP formation, one near 350 nm and another near 450 nm. For 5 nm evaporation thicknesses, a resonance near 450 nm exists before and after annealing. This suggests a discontinuous film morphology. AFM images confirm the formation of Ag nanoislands without any annealing for thin evaporations. Upon annealing, the particles making up the Ag layer become more uniform and the SP peak tightens. At 10 nm of Ag a very broad peak is visible before annealing and becomes well defined after annealing, showing both the dipole and quadrupole resonances.

Before annealing, the extinction spectra of 15 nm and 20 nm Ag films exhibit properties of the bulk material with no observed SP resonance. After the annealing a SP resonance is observed with a shift toward larger wavelength. Above 20 nm thickness, a distinct and consistent SP peak is difficult to attain. This limit suggests there is a critical thickness beyond which surface tension is unable to permit a uniform layer of NPs. For very thin silver films, it is possible to form SP modes between the top and bottom surfaces of the film.

However, the films above 10 nm exhibit bulk properties; thus we have a suitable mirror to compare the NP layer devices.

Electromagnetic theory accurately describes the SP resonance of metallic spheres by the Mie theory whereas more complicated shapes require more advanced electromagnetic theory, including dynamic modeling like the discreet dipole approximation. The dependencies of the SP resonance frequency on the dielectric properties of the surrounding medium and the diameter, ellipticity, and density of the NPs have already been described in detail [16,23–25]. As expected from theory, a redshift in the SP resonance is observed for thick LiF layers.

The transition from near-field coupling effects to far-field interference takes place at $\lambda/2\pi$. For the peak absorption wavelength of MEH-PPV, we expect a transition near 75 nm. In the near field, the enhancement in PL efficiency for the mirrored devices (device type 2) is a competition between quenching and reflection. While the number of quench sites remains constant for different Ag layer thicknesses, the amount of light reflected is related to the dielectric properties of the Ag layer. For NP devices (device type 3), the correlation is not as simple. In addition to the amount of reflected light, which should change due to the

Table 1
Relationship between Ag deposition thicknesses (T_{Ag}), the average of the resulting Ag NP diameters (D_{Ag}), and the observed SP resonance (λ_{SPR}) is displayed on the left of the table. On the right, the measured LiF thickness (T_{LiF}) and observed surface roughness of the LiF layer (LiF_{rms}) is given.

T_{Ag} (nm)	D_{Ag} (nm)	λ_{SPR} (nm)	T_{LiF} (nm)	LiF_{rms} (nm)
5	4.5	451	4.7	1.10
10	6.5	482	22	4.08
15	15	492	40	6.47
20	25	519	70	10.9

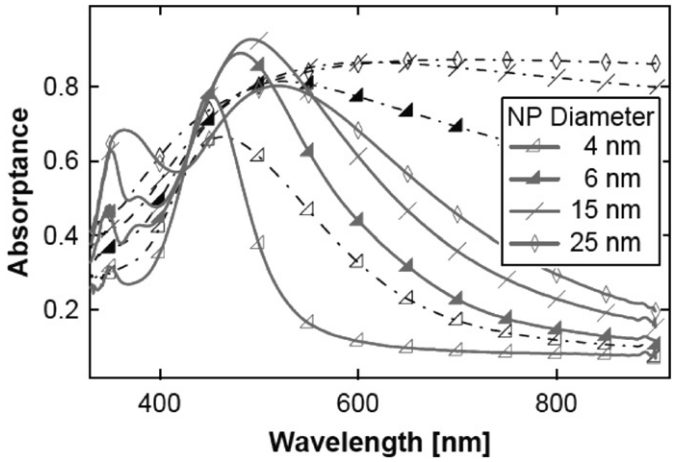

Fig. 3. Characterization of a thermally deposited Ag film before annealing (dashed black curves) shows a SP peak for the thinnest deposition of Ag. After annealing (solid gray curves), SP peaks are well formed for Ag deposition thicknesses up to 25 nm.

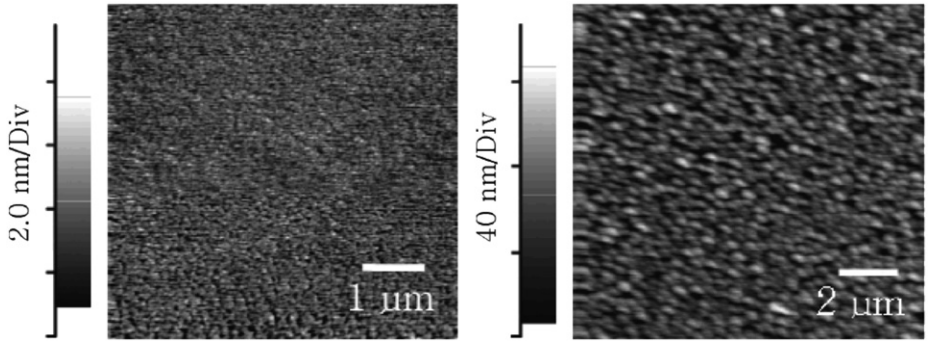

Fig. 2. Contact mode AFM image on the left shows the surface of the Ag layer before annealing. The image on the right shows the same Ag layer after annealing containing NPs with 25 nm heights. Left image has a 25 μm^2 area and the right has 100 μm^2 area.

modified dielectric dispersion, the SP evanescent field normal to the surface causes a dramatic change in the local electric field intensity. This modifies the absorption and emission rates of the adjacent fluorophore, resulting in PL enhancement. These large effects change the characteristics from the behavior of the mirrored devices to the high yields of the NP devices.

Fig. 4(a) shows the PL of mirrored devices for different Ag evaporation thicknesses with a fixed LiF spacer thickness of 20 nm and 40 nm thickness of MEH-PPV. For Ag thicknesses below 15 nm, quenching is dominant over reflection enhancement effects. But, as expected, we see larger enhancement as the Ag thickness increases. This is due to the change in optical properties of Ag because, for thicker layers, the extinction characteristics approach those of bulk Ag, causing more reflection (see Ref. [3]).

The curves in Fig. 4(b) show that Ag NP devices exhibit similar behavior to those of the mirrored devices, where a general increase in PL is seen for thicker layers (NP diameters) of Ag. In contrast however, the enhancements are much larger, with a maximum of 5:6 times the peak PL of device type 1. The smallest enhancements were found for SP resonances overlapping the absorption peak of MEH-PPV at 475 nm. PL emission was observed to increase for larger particles with resonances that have a larger overlap with the emission peak of MEH-PPV (observed at 575 nm). This result shows that the largest factor

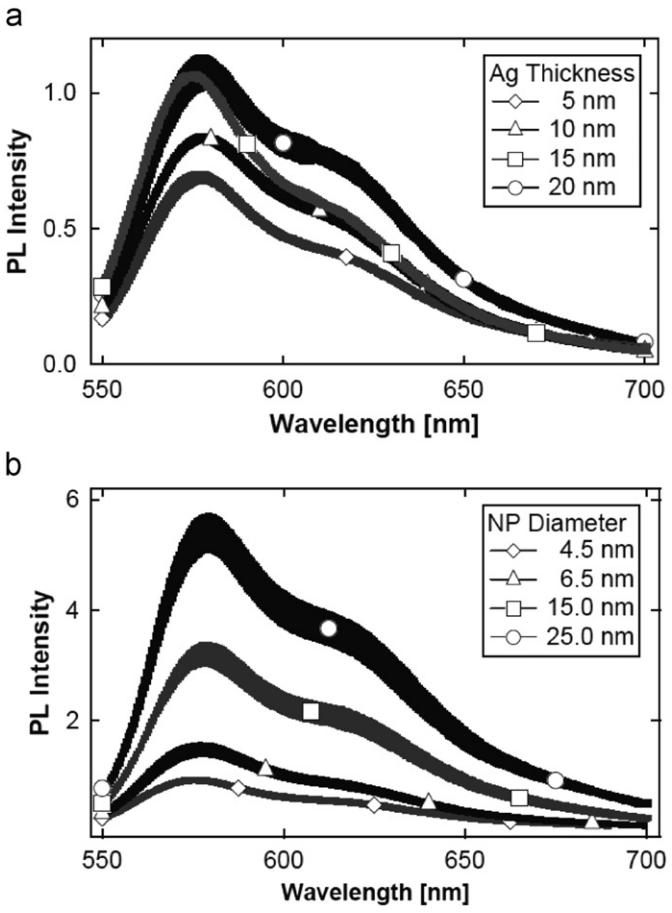

Fig. 4. PL dependence on Ag evaporation thicknesses is observed for a 475 nm excitation wavelength. Error bars, shown as line widths, were calculated from the variation over four duplicates of each mirror and NP device. The MEH-PPV and LiF spacer thicknesses for all devices are 40 and 20 nm, respectively. (a) PL of mirrored devices achieves a 7.5% increase over plain MEH-PPV/glass devices. (b) NP devices exhibit a large increase in light emission, up to 5.6 times that of plain MEH-PPV and 5.2 times that of the highest performing mirror device.

giving rise to the enhancements is not an enhancement of the light absorption but increasing of the fluorescent radiative rate caused by interaction with the SPs. While SP field effects should be spacer thickness dependent, scattering should be relatively constant in the near-field regime. The increase in detected emission was found to be dominated by SP effects through a spacer thickness dependence study, which is discussed in detail below.

We find similar results when comparing the integrated PL over the observed emission wavelengths ranging from 550 to 700 nm. The integrated PL of the 25 nm diameter NP devices compared to that of the control is 5.9 times larger. This 5% change over the peak PL enhancement suggests that there is only a slight change in PL spectral shape.

Overall enhancement is determined by the characteristic decay length of the SP field, the $1/r^4$ quenching distance dependence [26], and constant scattering off the NP layer. The evanescent electric field responsible for the increase in the quantum yield is expected to decay exponentially as $e^{-\beta z}$ where z is the depth of the penetration and β is given by the characteristic penetration depth π:

$$d_p = \frac{1}{\beta} = \frac{\lambda}{2\pi}\sqrt{\frac{\varepsilon_2-\varepsilon_1}{\varepsilon_1^2}}, \tag{2}$$

where λ is the excitation wavelength and $(\varepsilon_1, \varepsilon_2)$ are the real parts of the dielectric constant of the metal and the polymer, respectively [27]. A penetration depth of 43.3 nm is calculated for MEH-PPV and 40.6 nm for LiF. This compares well with a previous result for PMMA at 38.6 nm [26]. Fig. 5(a) shows the intensity of the electric field as it penetrates through the LiF and into the MEH-PPV, where both films are 40 nm thick.

Fig. 5(b) shows the distance dependence of the effects from the metallic films for both 15 nm thick mirrors and 15 nm diameter NPs. Quenching is the dominant effect for the mirrored devices (◆ curve) and it follows a similar shape seen before by Becker et al. [18]. The differences in shape can be attributable to the differences in material and the thicker MEH-PPV film used here. However, large enhancements in the NP devices (○ curve) are observed with a peak around 40 nm distance separation, which corresponds well with the calculated penetration depth. Both the distance dependence and the large enhancement confirm that surface enhanced fluorescence and not reflection is the dominant effect.

Absorptance measurements were taken and show less than a 10% change over the range of LiF thicknesses. This puts a limit on the effect the excitation intensity has, which suggests that the enhancement is due largely to an increase in the quantum efficiency. Similar work by Neal et al. [11] explains the increase by introducing a new term (k_{SP}) to the internal quantum efficiency (η^*_{int}) calculation:

$$\eta^*_{int} = \frac{k_{rad}+k_{SP}}{k_{rad}+k_{nonrad}+k_{SP}}, \tag{3}$$

where k_{rad} is the radiative recombination rate, k_{nonrad} is the nonradiative recombination rate, and k_{SP} is the recombination rate due to the plasmons. For large LiF spacer thicknesses k_{SP} is small and the PL of the control is expected for both NP and mirror devices. As the separation distance is made thinner k_{SP} increases which allows for enhancement. But for small spacer thicknesses the high transfer rate allows for saturation of the transfer to SP states and increases the cross-section for nonradiative recombination, resulting in lower PL enhancement.

The peak in PL enhancement around 40 nm LiF thickness is drastically different from that in the SP enhanced PL in fluorescent dyes such as rhodamine 6G, where the canonical separation

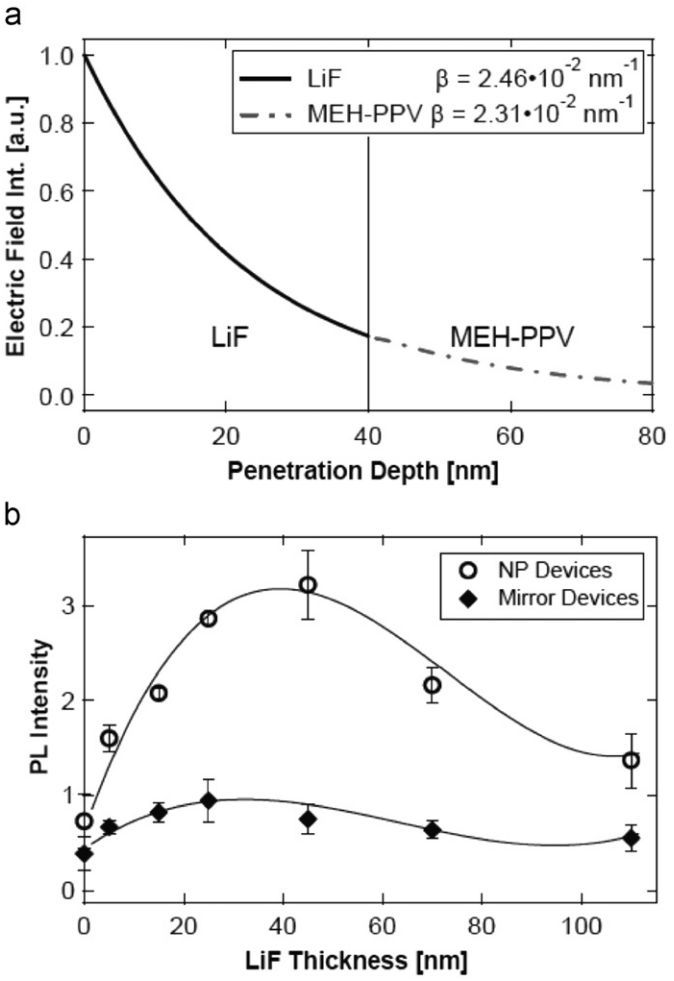

Fig. 5. (a) Solid curve shows the decay of the evanescent SP electric field intensity through the LiF optical spacer and the dashed curve shows the longer decay through the MEH-PPV. (b) Distance dependence of MEH-PPV PL to Ag NP layer and mirror is observed. The data are normalized to the peak PL of the control and a line is drawn to guide the eye. The data shown here are averaged over four devices with MEH-PPV and Ag deposition thicknesses of 40 and 15 nm, respectively. Error bars show the standard deviations in the data.

distance for dyes is approximately 5 nm [15,28]. This observed contradiction can be understood through the differences in the quenching distance dependence between dyes and polymers. Significant quenching in dyes takes place within 10 nm distance separation [29], whereas in polymers the separation range is out to 60 nm [18]. This agrees well with our findings, resulting in a larger separation distance for polymers before maximum enhancement takes place.

4. Summary

In summary, the work presented here shows that the PL of MEH-PPV is enhanced in the presence of Ag NPs for varying NP sizes and plasmon–fluorophore separation distances. PL enhancement was found for Ag NPs with diameters in the range of 6.5 to 25 nm with the largest enhancements for SP resonances near the emission peak of MEH-PPV. As we would expect within the near-field optical range, the difference in the mirrored and NP devices suggests that the large PL enhancement is not due to interference effects but due to a superposition of modification by the SP field and the change in the PL quantum efficiency.

The study of MEH-PPV PL for a range of separation distances found that PL enhancement reaches a maximum near 40 nm LiF thickness. This finding is strikingly different from the separations required for small molecule systems. The long chains of MEH-PPV are easily quenched along the entire chain length, which makes polymers more sensitive to PL quenching than small molecule systems and thus larger separation distances are required to achieve maximum PL enhancement. The SP field penetration depth indicated that a significant evanescent field existed within the MEH-PPV for enhancement in the LiF thickness range studied. Small changes in absorption were observed over a large LiF thickness range, indicating that radiative decay rates were affected and that the overall quantum efficiency was modified. Further investigations will be directed toward effects due to changing the molecular weight of the conjugated polymer, NP spacing, and time resolved PL to better understand the effects on the radiative decay rates.

Acknowledgment

Acknowledgment is made to the Donors of the American Chemical Society Petroleum Research Fund for partial support of this research.

References

[1] S. Nie, S.R. Emory, Science 275 (1997) 1102.
[2] S. Kuhn, U. Hakanson, L. Rogobete, V. Sandoghdar, Phys. Rev. Lett. 97 (4) (2006) 017402.
[3] R.R. Chance, A. Prock, R. Silbey, Advances in Chemical Physics, in: S.A.R.I. Prigogine (Ed.), John Wiley & Sons, Inc., 2007, pp. 1–65.
[4] Y. Chen, K. Munechika, I.J.-L. Plante, A.M. Munro, S.E. Skrabalak, Y. Xia, D.S. Ginger, App. Phys. Lett. 93 (3) (2008) 053106.
[5] O. K., N. I., S. A., N. Y., A. Mukai, T. Scherer, Physica Status Solidi C 2 (2005) 2841.
[6] S. Pillai, K.R. Catchpole, T. Trupke, M.A. Green, J. Appl. Phys. 101 (2007) 3105.
[7] A. Leitner, M.E. Lippitsch, S. Draxler, M. Riegler, F.R. Aussenegg, Appl. Phys. B 36 (1985) 105.
[8] S. Saini, S. Bhowmick, V.B. Shenoy, B. Bagchi, J. Photochem. Photobio. A: Chem. 190 (2007) 335 ISSN 1010-6030, theoretical Aspects of Photoinduced Processes in Complex Systems.
[9] G.D. Hale, J.B. Jackson, O.E. Shmakova, T.R. Lee, N.J. Halas, Appl. Phys. Lett. 78 (2001) 1502.
[10] H.J. Park, D. Vak, Y.Y. Noh, B. Lim, D.Y. Kim, Appl Phys. Lett. 90 (2007) 161107.
[11] T.D. Neal, K. Okamoto, A. Scherer, M.S. Liu, A.K.-Y. Jen, Appl. Phys. Lett. 89 (3) (2006) 221106.
[12] I.-S. Liu, Y.-F. Chen, W.-F. Su, J. Photochem. Photobio. A: Chem. 199 (2008) 291.
[13] M. Westphalen, U. Kreibig, J. Rostalski, H. Lth, D. Meissner, Sol. Energy Mater. Sol. Cells 61 (2000) 97.
[14] V. Sholin, J.D. Olson, S.A. Carter, J. Appl. Phys. 101 (9) (2007) 123114.
[15] J. Kummerlen, A. Leitner, H. Brunner, F.R. Aussenegg, W. A., Mol. Phys. 80 (1993) 1031.
[16] E. Hao, G.C. Schatz, J. Chem. Phys. 120 (2004) 357.
[17] Y. Chen, K. Munechika, D.S. Ginger, Nano Lett. 7 (2007) 690.
[18] H. Becker, S.E. Burns, R.H. Friend, Phys. Rev. B 56 (1997) 1893.
[19] K.H. Drexhage, Progr. Opt. 12 (1974) 165.
[20] N.C. Greenham, I.D.W. Samuel, G.R. Hayes, R.T. Phillips, Y.A.R.R. Kessener, S.C. Moratti, A.B. Holmes, R.H. Friend, Chem. Phys. Lett. 241 (1995) 89.
[21] D.S. Wang, M. Kerker, Phys. Rev. B 24 (1981) 1777.
[22] W.A. Weimer, M.J. Dyer, Appl. Phys. Lett. 79 (2001) 3164.
[23] G. Xu, M. Tazawa, P. Jin, S. Nakao, K. Yoshimura, Appl. Phys. Lett. 82 (2003) 3811.
[24] E.J. Zeman, G.C. Schatz, J. Phys. Chem. 91 (1987) 634.
[25] K.L. Kelly, E. Coronado, L.L. Zhao, G.C. Schatz, J. Phys. Chem. B 107 (2003) 668.
[26] B.N.J. Persson, N.D. Lang, Phys. Rev. B 26 (1982) 5409.
[27] T. Neal, K. Okamoto, A. Scherer, Opt. Express 13 (2005) 5522.
[28] J. Malicka, I. Gryczynski, Z. Gryczynski, J.R. Lakowicz, Anal. Biochem. 315 (2003) 57.
[29] A. Vaiana, H. Neuweiler, A. Schulz, J. Wolfrum, M. Sauer, J. Smith, J. Am. Chem. Soc. 125 (2003) 14564 ISSN 0002-7863.